Multimodal analysis of gas-oil intermittent structures in co-current horizontal flow

Stian Husevik Stavland
Department of Physics and Technology
University of Bergen
Bergen, Norway
Stian.Stavland@uib.no

Yessica Arellano
Fluids and Complex Systems Centre
Coventry University
Coventry, United Kingdom
prietoy@uni.coventry.ac.uk

Andy Hunt
Atout Process Limited
Brokenhurst, United Kingdom
andrew_hunt@atoutprocess.com

Rachid Maad
Department of Physics and Technology
University of Bergen
Bergen, Norway
Rachid.Maad@uib.no

Bjørn Tore Hjertaker
Department of Physics and Technology
University of Bergen
Bergen, Norway
Bjorn.Hjertaker@uib.no

***Abstract*— Multiphase flow measurement aims to accurately quantify the flow rates of the fluids flowing through a pipe. Depending on the measurement principle, the accuracy can be heavily affected by the spatial distribution of flow components. The component distributions or flow patterns vary depending on the fluid properties and process conditions. The present work reports the measurement principles and analysis of the data simultaneously acquired from a multimodal metering device. A combined multimodal analysis, encompassing hard and soft tomography techniques, potentially leads to enhanced accuracy of the flow fractions. The multimodal approach exploited here combines Gamma-Ray tomography (GRT) and Electric Capacitance tomography (ECT). The metering methodology combines the robustness and high resolution of the techniques for density stratification and permittivity distributions imaging. The fundamental principles and imaging capabilities of each technique are addressed here. First results of the multimodal approach performance are also demonstrated using intermittent flow structure data obtained from the multiphase flow loop at NORCE Technology. The challenges and potential improvements are also stated.**

Keywords*— *Multimodal tomography, multiphase flow, gamma-ray tomography, electrical capacitance tomography

I. INTRODUCTION

Within the Oil and Gas industry, hydrocarbon transport remains a challenge due to the intrinsic solubility of the production associated fluids and the wide range of process conditions throughout the production chain. Depending on the measurement principle, the accuracy of the flow meters has been found to be heavily affected by the fluid properties and process conditions. Multiphase flow measurement (MFM) is inherently complex leading to existing commercial devices with uncertainties from 5% to 20% or more on each of the flowing phases. This reality yields flow assurance issues and transport difficulties that challenge the downstream equipment operation.

Industrial Process Tomography (IPT) techniques have advantageous characteristics that make them highly attractive for MFM measurement. These characteristics answer to the requirements of the industry and address some key challenges in terms of process invasiveness, costs, speed, and capabilities to be adapted to vessels of various sizes. In this regards there is evidence of an increasing amount of interest in the research community for soft tomography systems targeting MFM when contrasted to the total number of investigations in other industrial fields [1]. Among these systems, we find Electrical Capacitance Tomography (ECT), a soft tomography technique that has been largely used for imaging and velocity measurement of non-conducting two-phase flows [2][3]. The applications of ECT concerning the Oil and Gas Industry, have proved highly accurate in oil-gas metering [4] [5] and mixtures with low water cuts [6].

Latest works in MFM comprise multi-modal and multi-spectral imaging methods that address various process monitoring including the use of dual-modality tomography to improve the typically low spatial resolution [7]. The present work correlates two-phase flow measurements from combined hard and soft tomographic metering technologies. This study explores the use of the multimodal approach, from cross-sectional reconstructed data, for measurement of dynamic multiphase flow patterns departing from previous experiences restricted to static structures [8].

Hard tomography based on radiation attenuation methods is well studied for determination of the gas fraction distribution non-intrusively in two-phase gas-liquid flows. These techniques are known to give reliable measurements in stratified gas-oil flows, and gas-solid flows [9][10]. Of the existing radiation attenuation methods, gamma-ray densitometry is less expensive than neutron-densitometry and offers monochromatic radiation without intensity fluctuations, contrary to X-ray attenuation techniques [11].

Hydrocarbon flow structures are contrasted here using, for the first time, a zonal sectorization procedure of the reconstructed images from gamma-ray tomography (GRT) and electrical capacitance tomography (ECT). This dual-modality combination is based on the measurement of different physical quantities of the fluids, i.e. density and electrical permittivity.

The present work aims to reduce the traditional meter limitations by combining measurement signals from a GRT and an ECT. The correlation of the measurements obtained through the arrays of sensors allows for the distribution of the components in the pipe. Hence, the combination of hard and soft tomography techniques offers the opportunity of enhanced metering accuracy to existing systems.

II. METHOD

A. Experimental facilities

The experiments were conducted at NORCE Technology in Bergen, Norway. A schematic of the flow loop showing the position of key components is shown in Fig. 1. The test facility comprises a recirculating three-phase pressurized flow loop with a gravimetric separator for separation of fluids in continuous operation. The phase separator has a 32 m^3 capacity, and typically contains around 10 m^3 of diesel and 10 m^3 of water.

In the tests, diesel and nitrogen gas were used as test fluids. The liquid flow was recirculated around the test facility using centrifugal pumps. The reference liquid flow rate was measured downstream of the pump using a Coriolis flow meter. The gas, supplied from a compressor facility, was added further downstream through a standard T connection. The gas flow rate was also measured using Coriolis flowmeters.

The rig is instrumented to provide reference measurements of phase fractions, flow rates, pressure and temperature of all fluids. The experiments were conducted at room temperature with fluid temperatures around 20 °C.

During the tests, the horizontal experimental section of 3" SCH160 was used. The loop was operated at 30 m^3/h and 30 m^3/h of gas and liquid respectively, which resulted in mean superficial velocities of 1.83 m/s and a mixture velocity of 3.66 m/s.

The diagram of the test section in Fig. 1 illustrates the relative positions of the GRT unit and the ECT sensors. The metering devices were located in the same horizontal section with the ECT sensor placed 1.2 m downstream the GRT measuring plane as shown in Fig. 2. Combined ECT and GRT measurements provide real-time flow imaging and continuous monitoring of the multiphase flow structures i.e., density, velocity and permittivity distributions that translate to in-situ volumetric fractions.

B. Gamma-ray Tomography

The high-speed gamma-ray tomograph is designed and prototyped at Department of Physics and Technology, University of Bergen. The design is based on five 500 mCi 241Am gamma-ray sources at a principal energy of 59.5 keV, symmetrically mounted around the pipe, as shown in Fig. 3. Corresponding to the five gamma-ray radiation sources, five detector arrays, each consisting of 17 CdZnTe detectors, are mounted on the opposite side of the pipe. CdZnTe semiconductor detectors offer a good signal-to-noise ratio and short response time, in addition to high stopping efficiency at the selected gamma-ray energy. The CdZnTe semiconductor detectors are operated in pulse mode, with a read-out system optimized for high count rates with a peaking time of only 200 ns [12].

The measurement is based on measuring the attenuation of the radiation through the media. In the gamma-ray energy range dominated by Compton scattering, the linear attenuation is approximately proportional to the density of the matter for monochromatic radiation.

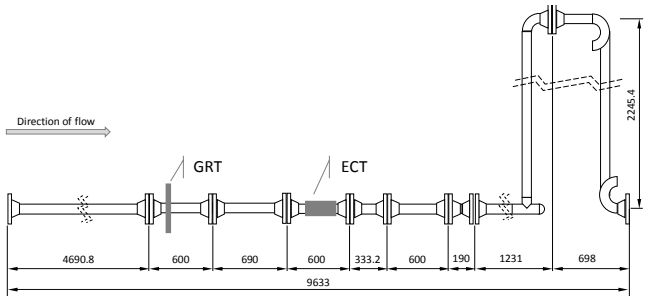

Fig. 1. Schematic of the test section at NORCE.
(Modified from: Test Protocol for Multiphase Intercomparison Roxar 2600 ID67mm Transfer Package, p5)

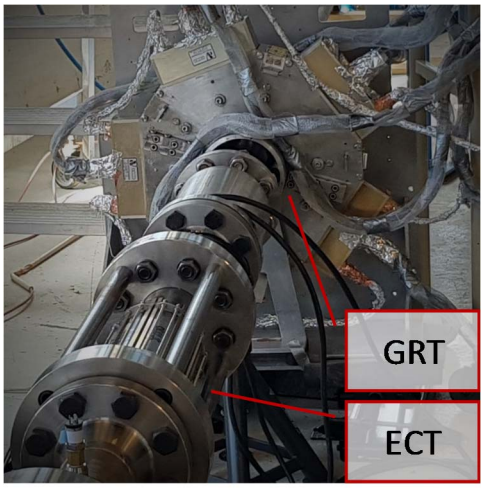

Fig. 2. Gamma-ray tomography (GRT) and electrical capacitance tomography (ECT) systems installed on the experimental test section

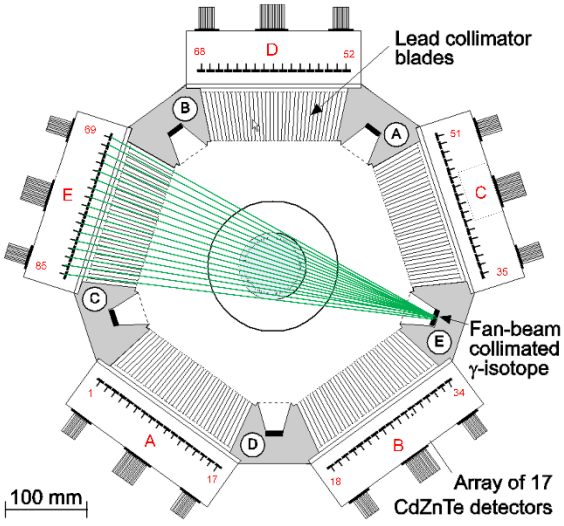

Fig. 3 High-speed gamma-ray tomograph. The notation A, B, C, D and E in the figure refers to gamma radiation source and detector array paires (views).

For a narrow beam the measured intensity I in relation to the incident beam intensity I_0, the build-up factor B, the linear attenuation μ and the distance x is given by the Beer-Lambert exponential decay law, as shown in (1) [13].

$$I = BI_0 e^{-\int \mu(x)dx} \quad (1)$$

The average linear attenuation can be found from taking the natural logarithm of the ratio I_0/I and dividing by the length the radiation travel through the medium. For mixtures and compounds, the average linear attenuation is the sum of the products between attenuation and volume fraction of each component assuming a distribution close to homogenous or layered perpendicular to the beam. This assumption generally holds for matter within a narrow beam.

For two component mixtures, it is often more convenient to measure the component fractions. This can be done by normalizing the measured intensity to that of the calibrated measured intensity of the single components, as shown in (2). Here, I_1 and I_2 are the measured intensities for the single components, α_1 is the volume fraction of the first component and I_m the measured intensity of the mixture.

$$\alpha_1 = \ln\frac{I_2}{I_m} \Big/ \ln\frac{I_2}{I_1} \tag{2}$$

This yields 85 independent line measurements of the component fractions that is used for the reconstruction of the fraction distribution across the cross section of the pipe.

C. Electrical Capacitance Tomography

The principle of operation of ECT is based on the sensitivity of the electrodes to changes in the dielectric properties of the fluids in the pipe. The difference between the permittivity of the components causes variations in the inter-electrode capacitance measurement. Each electrode-pair combination will have an associated sensitivity matrix containing N number of pixels. The elements in the sensitivity matrix for each electrode pair indicate whether a change in the permittivity of a single pixel inside the sensor will affect the capacitance measured between the electrodes of this pair. Hence, the measurements from the sensors are directly proportional to the distribution of the dielectric properties within the pipe. ECT measures the capacitances between unique combinations of pairs of electrodes placed around the perimeter of the pipe.

The sensor array used here, was arranged around the outside of the horizontal test section of the rig. The meter comprised 16 electrodes arranged in two measurement planes of 8 sensors each. All unique capacitance pairs were measured yielding a full set of measurements. The calibration of the ECT meter used single-phase flow of diesel and gas in the pipe for reference measurements. The excitation signal was a 24 V peak to peak square wave at 2.5 MHz.

The mean flow velocities are computed considering the transit time of the dynamic structures between the twin measurement planes. The flow velocity within the pipe cross-section at each point in time is calculated by correlating the instantaneous concentration of one plane with that in the other plane. In order to represent physically appropriate areas of the flow and perform a comprehensive analysis of the velocities, the measurements are grouped into zones containing a number of pixels, as detailed in the following sections.

The time shift between the signals from both sensors corresponds to the time it takes the flow to travel the known distance that separate the sensors. The cross-correlation velocity function ($R_{xy,i}$) is expressed as in (3).

$$R_{xy,i}(\tau) = \lim_{T\to\infty}\frac{1}{T}\int_0^T C_{1,i}(t)C_{2,i}(t+\tau)dt \tag{3}$$

Where $C_{1,i}(t)$ and $C_{2,i}(t)$ are the instantaneous concentrations in zone i in measurement planes 1 and 2, respectively. T is the averaging time.

D. Correlation of measurements

The comprehensive analysis of the flow obliged for the division of the pipe cross-section into zones, for each of which the individual phase fractions and velocities were computed. The zoned map comprised a 32 by 32-pixel matrix discretized into 13 zones (see Fig. 6).

The permittivity spatial distributions reconstructed from the ECT measurements were taken at a rate of 354 frames per second. Conversely, the sampling rate of the GRT is restricted to 50Hz. Hence for comparison purposes, during the postprocessing of the experimental data, the permittivity and velocity measurements were downsampled to match the fraction measurements from the GRT. Also, since the ECT and GRT measurements where not strictly synchronized, the measurements were correlated and adjusted in time for comparison. The authors corroborated that no relevant data or physical phenomena were missed through the exercise.

The ECT and GRT measurements are combined, as shown in (4), to estimate the gas and liquid flow rates and the zonal distribution of these over the pipe cross section.

$$Q_i = \sum_{k=1}^{K} Q_{ik} = \sum_{k=1}^{K} \alpha_{ik} v_{ik} A_k \tag{4}$$

Where Q_i is ith component volume flow rate, α_{ik} and v_{ik} is the ith component fraction and velocity in the kth zone and A_k is the area of the kth zone. The component fractions are estimated from the GRT measurements and the velocities from the ECT measurements. In this work, the flow rate estimations are based on the assumption of no-slip within each zone, hence the measured mix velocity is used for all components ($v_{mix\,k} = v_{1k} = v_{2k}$).

Since the flow rate of the ith component within each zone is a linear combination of the zonal velocity, component fraction, and area, the relative uncertainty contribution to the zonal flow rate from each variable is the same as the relative uncertainty of the variable. A full quantification of the uncertainty is beyond the scope of this work. However, it is relevant to understand the uncertainty contribution from the individual measurements.

When combining the uncertainties from individual zones it is probable that some of these are correlated. Assuming the area uncertainties are negligible, the combined uncertainties can be expressed as in (5) [14], where the uncertainties are marked u, the correlation factors r and the number of zones N.

$$\begin{aligned} u_{Q_i}{}^2 = \sum_{k=1}^{N}\sum_{m=1}^{N} A_k A_m \Big(&\alpha_{ik}\alpha_{im}u_{v_{ik}}u_{v_{im}}r(v_{ik},v_{im}) \\ &+ v_{ik}v_{im}u_{\alpha_{ik}}u_{\alpha_{im}}r(\alpha_{ik},\alpha_{im}) \\ &+ 2\alpha_{ik}v_{im}u_{v_{ik}}u_{\alpha_{im}}r(v_{ik},\alpha_{im})\Big) \end{aligned} \tag{5}$$

III. Results and Discussion

The reported results are derived from measurements with nominal flow rates of 30 m^3/h oil and 30 m^3/h gas. The measurements were acquired over a time interval of approximately 2 minutes. The reported mean values are estimated over this interval.

Fig. 4 contrasts the development of the cross-sectional permittivity measurement from the ECT with that of the oil fractions measured using the five source-detector-array pairs (views) of the GRT. The correlation between the measurements is readily evident. The pattern is identifiable as intermittent structures. Some differences are obvious i.e. the length and shape of structures, which reflects the evolution of the dynamic structures over the distance separating the metering systems. Differences in the time delay between the metering systems are also observable and is a result of varying flow velocity.

The flow is predominantly formed by high-frequency periodic structures particularly evident in the optical images in Fig. 5(a). The reconstructed images in Fig. 5(b) and (c) show variable flow with gas plugs visible at the top of the pipe, which are not evident in the photographs (see Fig. 5(a)). The oil concentration is mostly high with rapid excursions to low values. The structures observed are consistent with plug flow reported in [15][16].

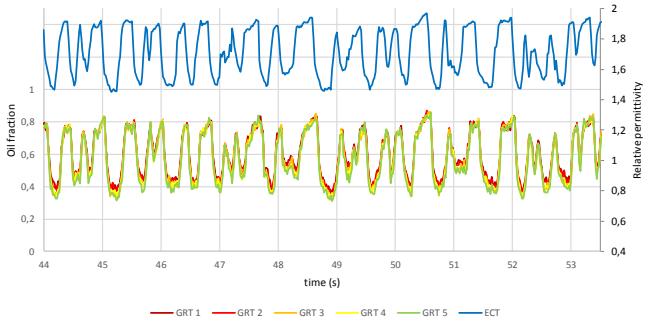

Fig. 4. Transient liquid fractions measured independently from each of the five source-detector-array pairs (views) of the gamma-ray tomography (GRT 1 to GRT 5) and relative permittivity measured with the electrical capacitance tomography (ECT).

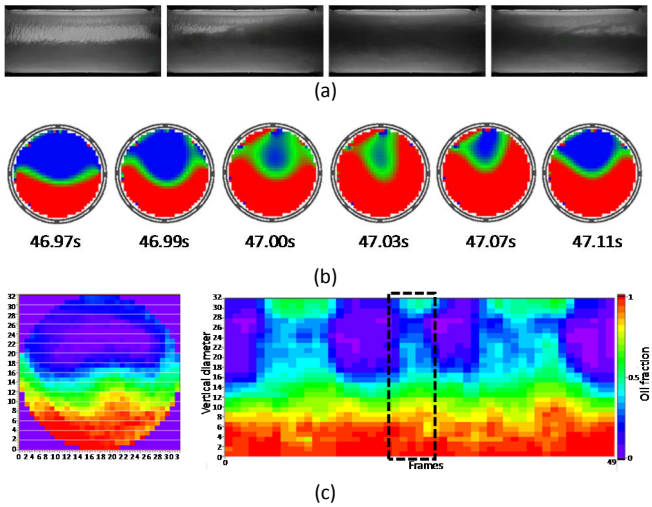

Fig. 5. Images of plug flow structures from (a) optical recordings (b) permittivity measurements through electrical capacitance tomography (ECT) and (c) density measurements from gamma-ray tomography with highlighted section corresponding to ECT reconstruction sequence above

ECT measurements on the average zonal velocity and the in-situ flow velocity are illustrated in Fig. 6 and Fig. 7, respectively. In Fig. 7(a) and Fig. 7(b) the instant flow velocity (right y-axis) is contrasted to the zonal oil fraction of the flow (left y-axis). The velocity measured at the top of the pipe is plotted in Fig. 7(a), this zone is where the gas pockets appear. It is evident that the flow velocity does not vary greatly throughout the testing period. At the top of the pipe, the instant flow velocity ranges between 6 and 7 m/s. However, no correlation was found between the dynamics of the structures and the velocity. Measurements at the bottom of the pipe, which is predominantly inundated with liquid, show a constant velocity at 4 m/s as evidenced in Fig. 7(b).

Flowrates were estimated from the combined instantaneous zonal velocity between the ECT planes and the corresponding fluid fractions from the GRT. Fig. 8 shows the mean zonal oil flowrate distribution in the pipe. Evidently, there are lower liquid fractions in the upper zones. The measured distribution in the upper zones results from the gas structures that intermittently travel at the top of the pipe. Similarly, Fig. 9 displays instantaneous oil and gas flowrates of a randomly selected time interval of 462 frames. The oil

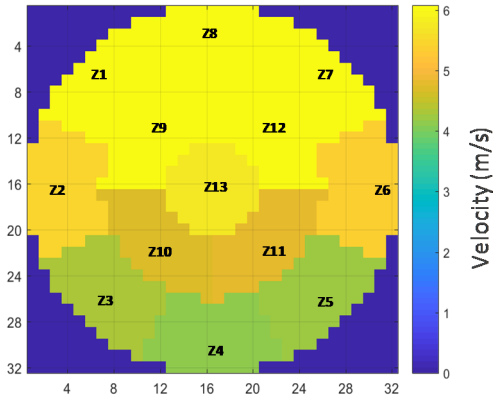

Fig. 6. Measurements from the electrical capacitance tomography system showing the reconstructed average velocity profile of the pipe cross-section

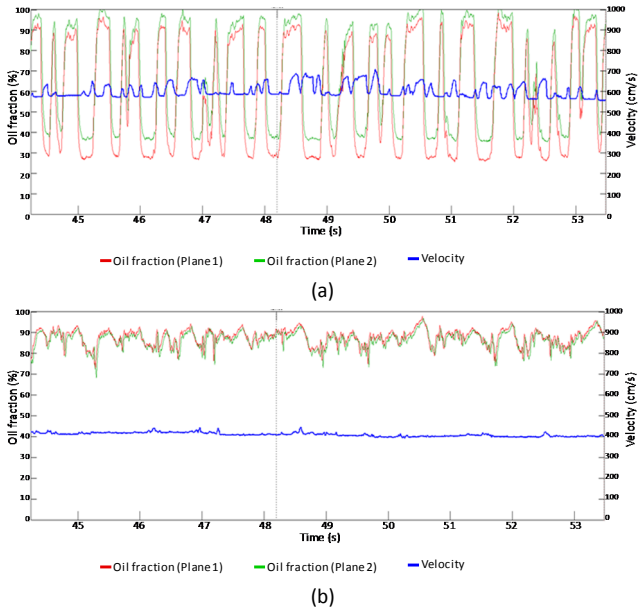

Fig. 7. Measurements from the electrical capacitance tomography system showing the flow velocity and oil fractions averaged over the zones situated (a) at the top of the pipe - Zone 8, and (b) at the bottom of the pipe - Zone 4.

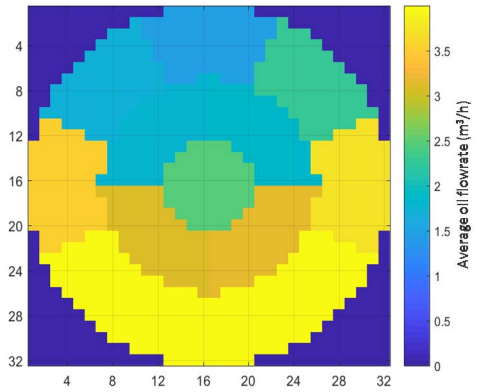

Fig. 8. Average oil flowrate computed for the zonal discretization from combined electrical capacitance tomography and gamma-ray tomography

flowrate in Fig. 9 follows the same trend evidenced in Fig. 4 and is inversely proportional to that of the gas phase.

The mean flow rate resulted in a mean value of 36.2 m^3/h for oil and 29.3 m^3/h for the gas phase in close relationship with the nominal inlet rates of 30 m^3/h for both components individually. The discrepancy among the nominal and measured values is thought to be associated with the cross-correlation velocity computation method. Where the slippage effect expected at the liquid-gas interphase in each zone is not considered in the zonal cross-correlation velocity measurements.

IV. Conclusions

In this work, two tomography techniques were combined to measure an oil-gas flow of 50% GLR. Permittivity measurements from an ECT were contrasted to the density distribution images reconstructed from GRT measurements. From both measurement systems, it was identified that the flow is predominantly dominated by high-frequency periodic structures characteristic of plug flow.

The multimodal approach showed agreement in the periodic structures measured. However, detailed comparison of the structures resulted in obvious differences in the length and the in-situ concentrations. Most likely a result of the evolution of the flow over the distance separating the metering systems. Velocity measurements were found to have little variation and no correlation with the plug flow dynamics. The combination of the measurements from both metering systems resulted in flow rate measurements in agreement with the reference inlet flowrates, particularly the gas flowrate. However, further analysis at different flowrates are needed to enhance the system correlation and measurement accuracy.

Some of the limitations of the present work comprise the distance between the sensor systems, which does not allow correlation of the flow structures, a matter that will be corrected in the future work.

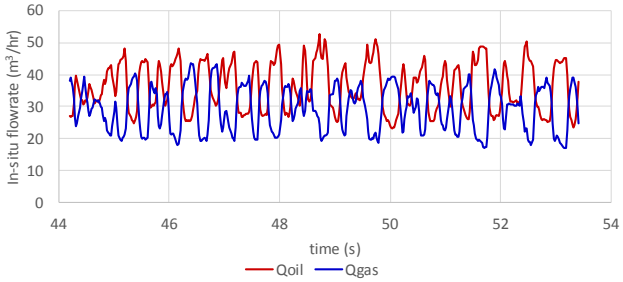

Fig. 9. Total gas and oil flowrates computed from the combinations of electrical capacitance tomography velocity measurements and phase fractions from gamma-ray tomography

Acknowledgment

This work was supported through the Joint Research Project MULTIFLOWMETII - Multiphase flow reference metrology. The project has received funding from the EMPR program co-financed by the Participating States and from the European Union's Horizon 2020 research and innovation program.

References

[1] Y. Arellano, O. Haas, H. Ahmed, A. Hunt, and L. Ma, "If cheap and easy oil is over, what nw?," in *International Cond=ference on energy and sustainable futures*, 2019, no. 1, pp. 1–7.

[2] M. Zhang, Y. Li, and M. Soleimani, "Experimental Study of Complex-valued ECT," in *9th World Congress on Industrial Process Tomography*, 2018, pp. 19–24.

[3] X. Zhu, P. Dong, and Z. Zhu, "Gas-solids Flow Measurement in Cyclone Dipleg by Dual-plane Electrical Capacitance Tomography Sensor," pp. 203–209, 2018.

[4] A. Hunt, L. A. Abdulkareem, and B. J. Azzopardi, "Measurement of Dynamic Properties of Vertical Gas-Liquid Flow," *7th Int. Conf. Multiph. Flow*, pp. 1–10, 2010.

[5] R. Yan and S. Mylvaganma, "Flow Regime Identification with Single Plane ECT Using Deep Learning," in *9th World Congress on Industrial Process Tomography*, 2018, pp. 289–297.

[6] A. Hunt, "Industrial Applications of High-speed Electrical Capacitance Tomography," in *9th World Congress on Industrial Process Tomography*, 2018, pp. 857–864.

[7] G. Liang, S. Ren, and F. Dong, "An Inclusion Boundary Reconstruction Method Using Electrical Impedance and Ultrasound Reflection Dual-Modality Tomography," in *9th World Congress on Industrial Process Tomography*, 2018, pp. 11–19.

[8] B. T. Hjertaker, R. Maad, and G. A. Johansen, "Dual-mode capacitance and gamma-ray tomography using the Landweber reconstruction algorithm," *Meas. Sci. Technol*, vol. 22, no. 104002, 2011.

[9] T. Dyakowski, G. A. Johansen, B. T. Hjertaker, D. Sankowski, V. Mosorov, and J. Wlodarczyk, "A Dual Modality Tomography System for Imaging Gas/Solids Flows," *Part. Part. Syst. Charact*, vol. 23, pp. 260–265, 2006.

[10] A. Hunt, J. Pendleton, and Y. Ladam, "Visualisation of two-phase gas-liquid pipe flows using electrical capacitance tomography," in *ESDA2004*, 2004, no. January 2004.

[11] S. H. Stavland, C. Sætre, B. T. Hjertaker, S.-A. Tjugum, A. Hallanger, and R. Maad, "Gas Fraction Measurements using Single and Dual Beam Gamma-Densitometry for Two Phase Gas- Liquid Pipe Flow," in *2019 IEEE International Instrumentation and Measurement Technology Conference (I2MTC)*, 2019, pp. 1–6.

EMPR program & European Union's Horizon 2020 research and innovation program.

[12] G. A. Johansen and E. Abro, “A new CdZnTe detector system for low-energy gamma-ray measurement,” *Sensors and Actuators*, vol. 54, no. 54, pp. 493–498, 1996.

[13] G. A. Johansen, *Radioisotope Gauges for Industral Process Measurements*. 2004.

[14] JCGM, “Evaluation of measurement data — Guide to the expression of uncertainty in measurement,” no. September. p. 134, 2008.

[15] J. Y. Lum, T. Al-Wahaibi, and P. Angeli, “Upward and downward inclination oil – water flows,” *Int. J. Multiph. Flow*, vol. 32, pp. 413–435, 2006.

[16] W. A. S. Kumara, B. M. Halvorsen, and M. C. Melaaen, “Pressure drop , flow pattern and local water volume fraction measurements of oil – water flow in pipes,” *Meas*, vol. 20, no. 114004, 2009.